ACS APPLIED MATERIALS & INTERFACES

Research Article

www.acsami.org

Control of Nanomorphology in All-Polymer Solar Cells via Assembling Nanoaggregation in a Mixed Solution

Wei Yu,[†,§] Dong Yang,[†,§] Xiaoguang Zhu,[‡] Xiuli Wang,[†] Guoli Tu,[‡] Dayong Fan,[†,§] Jian Zhang,*[,†] and Can Li*[,†]

[†]State Key Laboratory of Catalysis, Dalian Institute of Chemical Physics, Chinese Academy of Sciences, Dalian National Laboratory for Clean Energy, 457 Zhongshan Road, Dalian 116023, P. R. China

[‡]Wuhan National Laboratory for Optoelectronics, Huazhong University of Science and Technology, Wuhan, P. R. China

[§]Graduate University of Chinese Academy of Sciences, Beijing 100049, P. R. China

Supporting Information

ABSTRACT: The formation of interconnected phase-separated domains on sub-20 nm length scale is a key requirement for all-polymer solar cells (all-PSCs) with high efficiency. Herein, we report the application of crystalline poly(3-hexylthiophene) (P3HT) nanowires via an *O*-dichlorobenzene/hexane mixed solution blended with poly{(9,9-dioctylfluorenyl-2,7-diyl)-*alt*-[4,7-bis(3-hexylthiophen-5-yl)-2,1,3-benzothiadiazole]-2′,2″-diyl} (F8TBT) for the first time. The nanomorphology of P3HT:F8TBT all-PSCs can be controlled by P3HT nanowires. The improved film morphology leads to enhanced light absorption, exciton dissociation, and charge transport in all-PSCs, as confirmed by ultraviolet−visible absorption spectra, X-ray diffraction, transmission electron microscopy, atomic force microscopy, and time-resolved photoluminescence spectra. The P3HT nanowire:F8TBT all-PSCs could achieve a power conversion efficiency of 1.87% and a V_{oc} of 1.35 V, both of which are the highest values for P3HT:F8TBT all-PSCs. This work demonstrates that the semiconductor nanowires fabricated by the mixed solvents method is an efficient solution process approach to controlling the nanomorphology of all-PSCs.

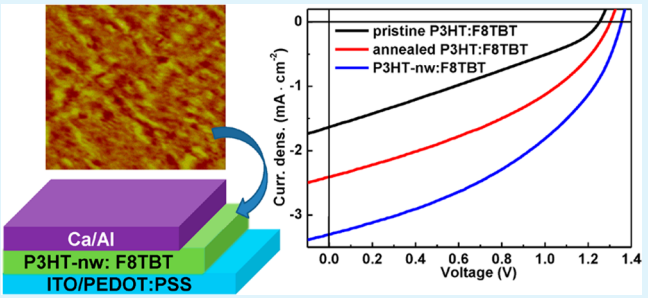

KEYWORDS: *all-polymer solar cell, nanomorphology, P3HT:F8TBT, nanoaggregation, mixed solvents*

INTRODUCTION

Polymer solar cells constitute a new promising approach to low-cost solar cells, because of their cost efficient processes through roll-to-roll technology.[1] All-polymer solar cells (all-PSCs) make up a class of polymer solar cells in which an n-type semiconducting polymer is used as the electron acceptor instead of a fullerene derivative. All-PSCs have some unique advantages over polymer/fullerene BHJs, such as high absorption coefficients in the visible spectral region and a large potential for fine tuning the energy levels because of the structural variety of polymers.[2−5] In addition, polymer/polymer blends offer superior flexibility in controlling solution viscosity, an important factor for film coating in large-scale roll-to-roll processes.[6] Although much less research has been devoted to all-PSCs, promising improvements in efficiencies to 3.3 and 3.6% have been reported recently.[7−12]

In all-PSCs, the efficiency is considered to be limited by the undesirable blend morphology,[2,13] such as the inhomogeneous internal phase composition,[14−18] the large phase separation,[19] and the poor ordering of polymer chains,[20] although researchers have attempted to improve the morphology of polymer blends with varied conditions, including the choice of solvents,[9] varying the molecular weight,[11] using a mixture of solvents,[12,21,22] processing aids,[23] thermal annealing treatment,[9,24] etc. However, none of these approaches allows full control over the film microstructure, in particular the interconnected pathways constructed by donor and acceptor materials. Geminate pair separation might be impeded by the intermixed morphology, and charge might be trapped by the randomly interspersed electron donor and acceptor phase. To further improve the efficiency, the interface of polymer blends needs to be as large as possible, while continuous pathways for dissociated charges to reach the electrodes must be maintained. This means that polymer domains should have a spacing size smaller than the exciton diffusion length, and the phase separation needs to be controlled at the nanometer scale.[25] The use of marginal solvents of *p*-xylene to construct P3HT [poly(3-hexylthiophene)] nanofibers in P3HT:F8BT [poly(9,9-dioctylfluorene)cobenzothiadiazole] films to control blend morphology has been reported. The morphology controlled by P3HT nanofibers increases the power conversion efficiency (PCE) of P3HT:F8BT PSCs to 0.055% in comparison with a value of 0.045% for thermally annealed

Received: October 11, 2013
Accepted: February 3, 2014
Published: February 3, 2014

   dx.doi.org/10.1021/am404483g | *ACS Appl. Mater. Interfaces* 2014, 6, 2350−2355

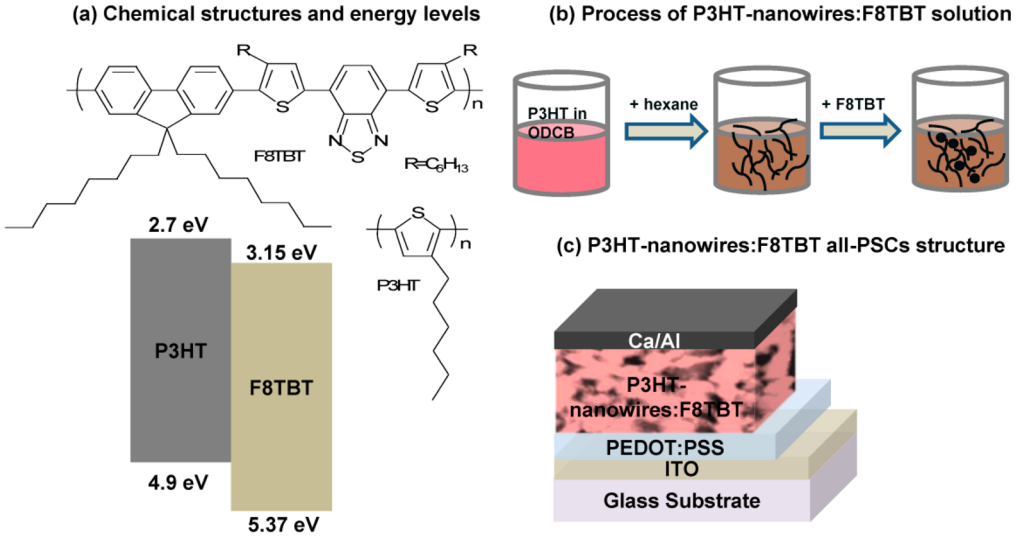

Figure 1. (a) Chemical structures and energy levels of P3HT and F8TBT. (b) Scheme illustrating the preparation of P3HT nanowire:F8TBT blend solutions via ODCB/hexane mixed solvents. (c) Device structures of P3HT nanowire:F8TBT all-polymer solar cells: glass/ITO/PEDOT:PSS/P3HT:F8TBT/Ca/Al.

devices.[26] Different from the P3HT:F8BT system, P3HT:F8TBT (poly{(9,9-dioctylfluorenyl-2,7-diyl)-*alt*-[4,7-bis(3-hexylthiophen-5-yl)-2,1,3-benzothiadiazole]-2′,2″-diyl}) all-PSCs can achieve a reasonable PCE of ∼1%,[20,27] and the PCE can be further improved to 1.85% by nanoimprinting technology to construct a nanostructured morphology with 25 nm features in P3HT:F8TBT all-PSCs.[28]

Via the addition of a poor solvent to the P3HT:PCBM-ODCB solution, polyalkylthiophene nanowires are constructed and applied in PSCs to control the morphology of composite films, which improves the device performance of P3HT:PCBM PSCs.[29,30] Herein, for the first time, we report the formation of P3HT nanowires in a mixed solution to control the nanomorphology of P3HT:F8TBT all-PSCs. The optimized phase-separated networks with lengths of 3−5 μm and ∼20 nm widths of P3HT nanowires are formed. Simultaneous improvements in the short circuit current (J_{sc}), open circuit voltage (V_{oc}), and fill factor (FF) are realized in P3HT nanowire:F8TBT all-PSCs. The average PCE of 1.87% and the V_{oc} of 1.35 V are the highest values for P3HT:F8TBT all-PSCs.

RESULTS AND DISCUSSION

Figure 1a presents the chemical structures of P3HT and F8TBT, along with their energy levels taken from the literature.[20] The preparation processes of P3HT nanowire:F8TBT blend solution via ODCB/hexane mixed solvents are shown in Figure 1b. The P3HT:F8TBT all-PSCs fabricated via the spin-coating process consist of the following structures: glass/ITO/PEDOT:PSS/P3HT:F8TBT/Ca/Al (Figure 1c). Except for the pristine P3HT:F8TBT films, the annealed P3HT:F8TBT and P3HT nanowire:F8TBT films were baked at 140 °C for 15 min in a glovebox before electrode deposition.

Figure 2a shows the current density−voltage (J−V) curves of pristine P3HT:F8TBT, annealed P3HT:F8TBT, and P3HT nanowire:F8TBT all-PSCs under simulated AM1.5G solar light illumination with an intensity of 100 mW cm^{-2}. For the P3HT nanowire:F8TBT devices fabricated from an ODCB/hexane mixed solution, J_{sc} increased from 1.62 to 3.20 mA cm^{-2}, FF from 0.30 to 0.42, and V_{oc} from 1.25 to 1.35 V in comparison with the values of the pristine devices prepared from an ODCB solution.

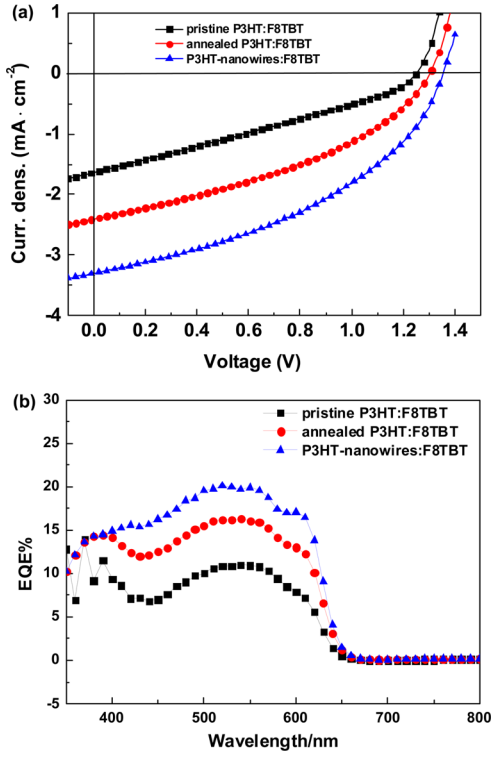

Figure 2. (a) Current density−voltage (J−V) curves of P3HT:F8TBT devices. (b) IPCE values of corresponding devices.

Table 1. Device Parameters of the Glass/ITO/PEDOT:PSS/P3HT:F8TBT/Ca/Al Devices Presented in Figure 2a

	J_{sc} (mA cm^{-2})	V_{oc} (V)	FF	η%
pristine	1.62	1.25	0.30	0.61
annealed	2.41	1.30	0.38	1.19
nanowires	3.29	1.35	0.42	1.87

As a result, the PCE is improved from 0.61% for the pristine devices to 1.87% for P3HT nanowire:F8TBT devices. The PCE of P3HT nanowire:F8TBT all-PSCs is among the highest reported for a P3HT:F8TBT system, which is comparable to the

dx.doi.org/10.1021/am404483g | ACS Appl. Mater. Interfaces 2014, 6, 2350−2355

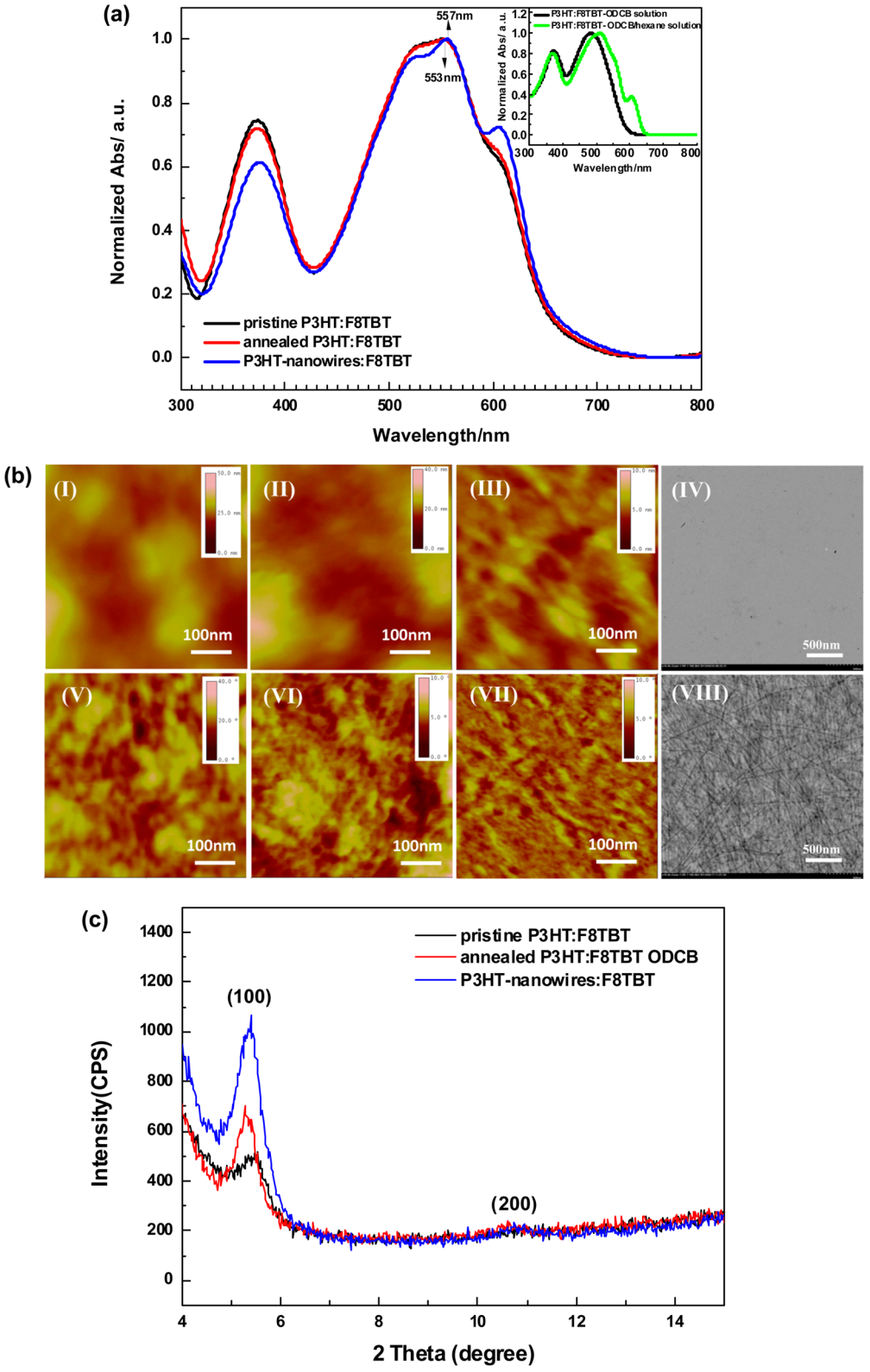

Figure 3. (a) UV−vis absorption of P3HT:F8TBT films fabricated from ODCB and an ODCB/hexane mixed solution. The inset shows the absorption of P3HT:F8TBT solutions in ODCB and ODCB/hexane solvents. (b) Atomic force microscopy (AFM) and transmission electron microscopy (TEM) images of P3HT:F8TBT and P3HT nanowire:F8TBT films. Panels I and V are AFM images of P3HT:F8TBT pristine films. Panels II and VI are AFM images of P3HT:F8TBT annealed films. Panels III and VII are AFM images of P3HT nanowire:F8TBT films. Panels IV and VIII are TEM images of films from a P3HT:F8TBT-ODCB solution and a P3HT:F8TBT-ODCB/hexane mixed solution, respectively. (c) X-ray diffraction patterns of P3HT:F8TBT films from ODCB and ODCB/hexane mixed solvents. All the films have a comparable thickness of ∼80 nm.

value of 1.85% of double-nanoimprinted P3HT:F8TBT all-PSCs with a feature size of 25 nm.[28] The thermally annealed P3HT:F8TBT devices at 140 °C for 15 min give an average PCE of 1.19% (V_{oc} = 1.30 V, J_{sc} = 2.41 mA cm^{-2}, and FF = 0.38),

dx.doi.org/10.1021/am404483g | ACS Appl. Mater. Interfaces 2014, 6, 2350−2355

which is also lower than that of P3HT nanowire:F8TBT all-PSCs. A detailed comparison of these parameters is given in Table 1. The statistical distribution of the device parameters is given in Figure S1 of the Supporting Information.

In comparison with the values of thermally annealed P3HT:F8TBT all-PSCs, the simultaneous improvements in J_{sc}, V_{oc}, and FF are seen for P3HT nanowire:F8TBT all-PSCs. The V_{oc} shows a mild improvement, and the value of 1.35 V is the highest for polymer solar cells in the single-junction configuration. The XPS spectra of N1s of the P3HT nanowire:F8TBT and thermally annealed P3HT:F8TBT films are presented in Figure S2 of the Supporting Information. P3HT has been found to preferentially wet the free surface in P3HT:F8TBT blends because of its low surface energy, which can serve as a blocking layer for the transport of an electron to the cathode and decrease the V_{oc}.[31] The formation of P3HT nanowires reduces the level of P3HT enrichment at the top cathode and then improves the V_{oc}.[32] To fully understand the origin of the higher V_{oc} in P3HT nanowire:F8TBT devices, more experiments will be needed, including determination of the inner structure of active layers by the XRR technique.[33,34]

The spectral dependence of the incident photon-to-current conversion efficiency, shown in Figure 2b, confirms that the enhanced PCE of P3HT nanowire:F8TBT all-PSCs is dominated by J_{sc}. In PSCs, J_{sc} is affected by light absorption, exciton dissociation, charge transport, and charge extraction processes. Figure 3a shows the UV−vis absorption spectra of the P3HT:F8TBT solution and films. The optical absorption spectra of the P3HT:F8TBT solution and films are a superposition of those of P3HT (Figure S3a of the Supporting Information) and F8TBT (Figure S3b of the Supporting Information). For the P3HT:F8TBT-ODCB solution in the inset figure of Figure 3a, only two bands at 372 nm (typical absorption band for F8TBT) and 484 nm (superposition of P3HT at 465 nm and F8TBT at 520 nm) can be resolved. Upon the addition of hexane into the well-dissolved P3HT-ODCB solution, two additional absorption bands at 558 and 607 nm appear in the P3HT:F8TBT-ODCB/hexane solution, and their intensity becomes stronger with an increase in the hexane concentration (Figure S4 of the Supporting Information). The amount of P3HT nanowires increases with an increase in the hexane concentration (Figure S5 of the Supporting Information). For the composite films (Figure 3a), the absorption associated with the F8TBT component is almost the same; however, as a result of preformed P3HT nanowires in a mixed solution, a slightly red shift of the absorption maximum from ∼553 to ∼557 nm and a large increase in the intensity of a shoulder band at ∼607 nm are observed for P3HT nanowire:F8TBT films. The red shift indicates an increase in the conjugation length in the P3HT nanowire:F8TBT film with a higher P3HT crystallinity.

Figure 3b shows the topography images and phase images of pristine P3HT:F8TBT, annealed P3HT:F8TBT, and P3HT nanowire:F8TBT films. The transmission electron microscopy (TEM) images of P3HT:F8TBT and P3HT nanowire:F8TBT films from a P3HT:F8TBT-ODCB solution and a P3HT:F8TBT-ODCB/hexane mixed solution are also shown in Figure 3b. Numerous homogeneously distributed P3HT nanowires with lengths of ∼5 μm and widths of ∼20 nm are observed in the TEM image of the P3HT nanowire:F8TBT film (Figure 3b, panel VIII), while no nanowire-like aggregations are observed in the TEM image of the P3HT:F8TBT film (Figure 3b, panel IV). The preformed nanowires can also be observed in the atomic force microscopy (AFM) images of the P3HT nanowire:F8TBT films (Figure 3b, panels III and VII), which are different from the AFM images of the P3HT:F8TBT films (Figure 3b, panels I and V and panels II and VI). The enhancement of the crystallinity of P3HT nanowire:F8TBT films is further proven by X-ray diffraction, as shown in Figure 3c. One main peak at a 2θ of ∼5.4° could be resolved for all the P3HT:F8TBT films and P3HT-only films (Figure S6 of the Supporting Information). This peak is assigned to the diffraction of the (100) plane of P3HT crystals. The P3HT:F8TBT pristine film has the lowest crystallinity. After the films are thermally annealed, the intensity of this main peak is increased and the peak width at half-height is decreased for the increased crystallinity of annealed P3HT.[35] For the P3HT nanowire:F8TBT films, the intensity of this peak is significantly enhanced, giving a slightly decreased d spacing (1.64 nm) of the (100) plane (vs 1.67 nm). These features are associated with an increased level of P3HT molecular order in films and show that the crystallinity of P3HT in the composite films has been substantially increased. The AFM images, TEM images, and X-ray diffraction (XRD) spectra indicate higher crystallinity and optimized nanomorphology in P3HT nanowire:F8TBT films that could improve J_{sc} and FF.[20]

Figure 4 shows the time-resolved photoluminescence spectra of P3HT:F8TBT films. The average lifetime of the pristine

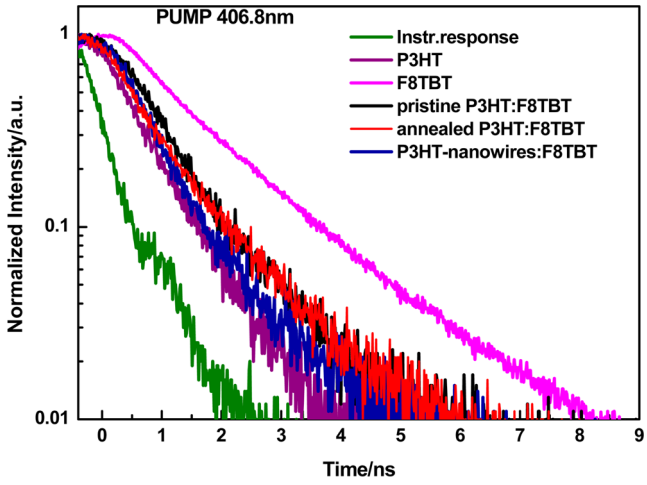

Figure 4. Profiles of the photoluminescence decay kinetics of pure P3HT, F8TBT films, and P3HT:F8TBT blended films.

P3HT:F8TBT film is 0.84 ns and that of the annealed P3HT:F8TBT film 0.78 ns, while the P3HT nanowire:F8TBT film photoluminescence decay is accelerated (0.70 ns). The shorter lifetime of the P3HT nanowire:F8TBT film indicates more efficient charge dissociation in the P3HT nanowire:F8TBT film.[20,36] It is well known that desirable phase-separated networks and the crystallization of P3HT after thermal annealing play a crucial role in the high efficiency of charge dissociation and collection.[37] Therefore, the charge dissociation of the P3HT nanowire:F8TBT film is improved by the optimized phase-separated networks.

CONCLUSIONS

In summary, we have shown that P3HT nanowire:F8TBT all-PSCs achieved a PCE of 1.87% with a V_{oc} of 1.35 V, the best performance yet reported for P3HT:F8TBT all-PSCs. The combined factors of broader absorption, improved surface properties, higher crystallinity, and optimized nanomorphology contributed to the improved performances. The crystalline

dx.doi.org/10.1021/am404483g | ACS Appl. Mater. Interfaces 2014, 6, 2350−2355

P3HT nanowires in a ODCB/hexane mixture solution allows pure, ordered, and interpenetrating domains at a 20 nm length scale to be formed through the active layers. The nanometer-scale phase separation in P3HT nanowire:F8TBT films is desirable for all-PSCs because of the avoidance of locally trapped photogenerated charges in the annealed polymer blends. The mixed solvent method could be extended to other crystalline polymers and provides an efficient way to assemble all-PSCs with high efficiency.

EXPERIMENTAL METHODS

Preparation of a P3HT Nanowire:F8TBT Solution. P3HT (synthesized in the laboratory) was dissolved in *o*-dichlorobenzene (ODCB, anhydrous, purchased from Sigma-Aldrich Co. Ltd.) at a concentration of 8.0 mg mL^{-1} to form a well-dissolved P3HT-ODCB solution. The P3HT nanowire solution was prepared by slowly and gradually adding a poor solvent of *n*-hexane to the P3HT-ODCB solution while it was being gently stirred.[27] The optimized ODCB/hexane ratio was 1/0.55 (v/v). Then the P3HT-ODCB/hexane solution was continuously gently stirred for 24 h. After that, F8TBT (M_w = 51000, polydispersity of 2.3, purchased from 1-Material) with a P3HT/F8TBT ratio of 1/1 (w/w) was added to the P3HT nanowire solution to form the P3HT nanowire:F8TBT solution. The P3HT:F8TBT-ODCB solution was prepared with a 1/1 (w/w) ratio at a total concentration of 16 mg mL^{-1} while being stirred at 60 °C for overnight.

Device Fabrication. All the devices were fabricated through a spin-coating process with a glass/ITO/PEDOT:PSS/P3HT:F8TBT/Ca/Al architecture (Figure 1c). First, an ∼50 nm thick PEDOT:PSS (Clevios 4083, purchased from H. C. Starck) layer was spin-coated onto the well-cleaned, O_2 plasma-treated ITO substrates. After being annealed on a hot plate at 150 °C for 15 min in air, the photoactive layers deposited from the prepared P3HT:F8TBT composite solution were spin-coated. No filtration was conducted for nanowire solutions, while the ODCB-only solutions were filtered with a 0.22 μm filter. The thickness of the photoactive layer was ∼80 nm, as determined by a Bruker 150 surface profiler for all the devices. Except for the pristine P3HT:F8TBT film, annealed P3HT:F8TBT and P3HT nanowire:F8TBT films were baked at 140 °C for 15 min in a glovebox before being transferred to the vacuum chamber for the evaporation of 10 nm Ca and 100 nm Al. The metal electrodes were thermally evaporated at $<5 \times 10^{-4}$ Pa with an area of 0.066 cm^2 defined by a metal mask. At least 100 devices were fabricated for each type of solar cell, and the performance given in the article is the average efficiency.

Characterization. A computer-controlled Keithley 2400 source measure unit was used to characterize the *J*−*V* performance of devices with an AM 1.5G Oriel solar simulator at an illumination intensity of 100 mW cm^{-2}. The corresponding external quantum efficiency was characterized on a QTest Station 2000ADI system (Crowntech Inc.). The films thickness of ∼80 nm was determined by a Bruker 150 surface profiler. The UV−vis absorption spectra were recorded on a Cary 5000 UV-Vis-NIR spectrophotometer. The XRD analysis conducted with an X-ray diffractometer (Rigaku) using Cu Kα radiation provided applied current and voltage values of 200 mA and 40 kV, respectively. TEM images were recorded with an HT7700-Hitachi instrument with an acceleration voltage of 100 kV. Tapping-mode AFM with height and phase images was conducted using a Bruker Metrology Nanoscope III-D atomic force microscope. Time-resolved photoluminescence spectra were recorded on an FLS920 fluorescence spectrometer (Edinburgh Instruments) in air at room temperature. A picosecond pulsed diode laser (406.8 nm) with a pulse width of 64.2 ps was used as the excitation source.

ASSOCIATED CONTENT

Supporting Information

Statistical distribution of device parameters, XPS spectra of N1s, UV−vis absorption spectra of P3HT and F8TBT, TEM images of P3HT nanowires at different ODCB/hexane ratios (v/v), XRD of P3HT films, and AFM images of P3HT and P3HT nanowires. This material is available free of charge via the Internet at http://pubs.acs.org.

AUTHOR INFORMATION

Corresponding Authors

*E-mail: jianzhang@dicp.ac.cn.
*E-mail: canli@dicp.ac.cn.

Notes

The authors declare no competing financial interest.

ACKNOWLEDGMENTS

This work was financially supported by the National Natural Science Foundation of China via Grants 20904057 and 21374120. J.Z. acknowledges the support of the 100 Talents Program of the Chinese Academy of Sciences.

REFERENCES

(1) Krebs, F. C.; Nielsen, T. D.; Fyenbo, J.; Wadstrom, M.; Pedersen, M. S. *Energy Environ. Sci.* **2010**, *3*, 512−525.
(2) McNeill, C. R.; Greenham, N. C. *Adv. Mater.* **2009**, *21*, 3840−3850.
(3) Zhan, X.; Tan, Z.; Domercq, B.; An, Z.; Zhang, X.; Barlow, S.; Li, Y.; Zhu, D.; Kippelen, B.; Marder, S. R. *J. Am. Chem. Soc.* **2007**, *129*, 7246−7247.
(4) Tan, Z.; Zhou, E.; Zhan, X.; Wang, X.; Li, Y.; Barlow, S.; Marder, S. R. *Appl. Phys. Lett.* **2008**, *93*, 073309−073311.
(5) Sang, G.; Zou, Y.; Huang, Y.; Zhao, G.; Yang, Y.; Li, Y. *Appl. Phys. Lett.* **2009**, *94*, 193302−193304.
(6) Facchetti, A. *Chem. Mater.* **2011**, *23*, 733−758.
(7) Earmme, T.; Hwang, Y.; Murari, N. M.; Subramaniyan, S.; Jenekhe, S. A. *J. Am. Chem. Soc.* **2013**, *135*, 14960−14963.
(8) Zhou, E.; Cong, J.; Hashimoto, K.; Tajima, K. *Adv. Mater.* **2013**, 6991−6996.
(9) Mori, D.; Benten, H.; Kosaka, J.; Ohkita, H.; Ito, S.; Miyake, K. *ACS Appl. Mater. Interfaces* **2011**, *3*, 2924−2927.
(10) Holcombe, T. W.; Woo, C. H.; Kavulak, D. F. J.; Thompson, B. C.; Freéchet, J. M. J. *J. Am. Chem. Soc.* **2009**, *131*, 14160−14161.
(11) Mori, D.; Benten, H.; Ohkita, H.; Ito, S.; Miyake, K. *ACS Appl. Mater. Interfaces* **2012**, *4*, 3325−3329.
(12) Zhou, E.; Cong, J.; Wei, Q.; Tajima, K.; Yang, C.; Hashimoto, K. *Angew. Chem., Int. Ed.* **2011**, *50*, 2799−2803.
(13) Sonar, P.; Fong Lim, J. P.; Chan, K. L. *Energy Environ. Sci.* **2011**, *4*, 1558−1574.
(14) Snaith, H. J.; Arias, A. C.; Morteani, A. C.; Silva, C.; Friend, R. H. *Nano Lett.* **2002**, *2*, 1353−1357.
(15) Shikler, R.; Chiesa, M.; Friend, R. H. *Macromolecules* **2006**, *39*, 5393−5399.
(16) McNeill, C. R.; Watts, B.; Thomsen, L.; Belcher, W. J.; Greenham, N. C.; Dastoor, P. C.; Ade, H. *Macromolecules* **2009**, *42*, 3347−3352.
(17) Swaraj, S.; Wang, C.; Yan, H.; Watts, B.; Lüning, J.; McNeill, C. R.; Ade, H. *Nano Lett.* **2010**, *10*, 2863−2869.
(18) Moore, J. R.; Albert-Seifried, S.; Rao, A.; Massip, S.; Watts, B.; Morgan, D. J.; Friend, R. H.; McNeill, C. R.; Sirringhaus, H. *Adv. Energy Mater.* **2011**, *1*, 230−240.
(19) Arias, A. C.; MacKenzie, J. D.; Stevenson, R.; Halls, J. J. M.; Inbasekaran, M.; Woo, E. P.; Richards, D.; Friend, R. H. *Macromolecules* **2001**, *34*, 6005−6013.
(20) McNeill, C. R.; Abrusci, A.; Hwang, I.; Ruderer, M. A.; Müller-Buschbaum, P.; Greenham, N. C. *Adv. Funct. Mater.* **2009**, *19*, 3103−3111.
(21) Campbell, A. R.; Hodgkiss, J. M.; Westenhoff, S.; Howard, I. A.; Marsh, R. A.; McNeill, C. R.; Friend, R. H.; Greenham, N. C. *Nano Lett.* **2008**, *8*, 3942−3947.
(22) Schubert, M.; Dolfen, D.; Frisch, J.; Roland, S.; Steyrleuthner, R.; Stiller, B.; Chen, Z.; Scherf, U.; Koch, N.; Facchetti, A.; Neher, D. *Adv. Energy Mater.* **2012**, *2*, 369−380.
(23) Liu, X.; Huettner, S.; Rong, Z.; Sommer, M.; Friend, R. H. *Adv. Mater.* **2012**, *24*, 669−674.
(24) McNeill, C. R.; Westenhoff, S.; Groves, C.; Friend, R. H.; Greenham, N. C. *J. Phys. Chem. C* **2007**, *111*, 19153−19160.
(25) McNeill, C. R. *Energy Environ. Sci.* **2012**, *5*, 5653−5667.

(26) Salim, T.; Sun, S.; Wong, L. H.; Xi, L.; Foo, Y. L.; Lam, Y. M. *J. Phys. Chem. C* **2010**, *114*, 9459−9468.
(27) Yan, H.; Collins, B. A.; Gann, E.; Wang, C.; Ade, H.; McNeill, C. R. *ACS Nano* **2012**, *6*, 677−688.
(28) He, X.; Gao, F.; Tu, G.; Hasko, D.; Hüttner, S.; Steiner, U.; Greenham, N. C.; Friend, R. H.; Huck, W. T. S. *Nano Lett.* **2010**, *10*, 1302−1307.
(29) Moulé, A. J.; Meerholz, K. *Adv. Mater.* **2008**, *20*, 240−245.
(30) Li, L.; Lu, G.; Yang, X. *J. Mater. Chem.* **2008**, *18*, 1984−1990.
(31) McNeill, C. R.; Halls, J. J. M.; Wilson, R.; Whiting, G. L.; Berkebile, S.; Ramsey, M. G.; Friend, R. H.; Greenham, N. C. *Adv. Funct. Mater.* **2008**, *18*, 2309−2321.
(32) Chen, D.; Nakahara, A.; Wei, D.; Nordlund, D.; Russell, T. P. *Nano Lett.* **2011**, *11*, 561−567.
(33) Guo, S.; Ruderer, M. A.; Rawolle, M.; Körstgens, V.; Birkenstock, C.; Perlich, J.; Müller-Buschbaum, P. *ACS Appl. Mater. Interfaces* **2013**, *5*, 8581−8590.
(34) Ruderer, M. A.; Guo, S.; Meier, R.; Chiang, H.; Körstgens, V.; Wiedersich, J.; Perlich, J.; Roth, S. V.; Müller-Buschbaum, P. *Adv. Funct. Mater.* **2011**, *21*, 3382−3391.
(35) Yang, X. N.; Loos, J.; Veenstra, S. C.; Verhees, W. J. H.; Wienk, M. M.; Kroon, J. M.; Michels, M. A. J.; Janssen, R. A. J. *Nano Lett.* **2005**, *5*, 579−583.
(36) Kim, Y.; Cook, S.; Choulis, S. A.; Nelson, J.; Durrant, J. R.; Bradley, D. D. C. *Chem. Mater.* **2004**, *16*, 4812−4818.
(37) Guo, J.; Ohkita, H.; Benten, H.; Ito, S. *J. Am. Chem. Soc.* **2010**, *132*, 6154−6164.